Prof. Sergio Tattoni – Università di Cagliari - DICAAR

"Exceptional actions: blast loads on reinforced concrete structures"

EXCEPTIONAL ACTIONS: BLAST LOADS ON REINFORCED CONCRETE STRUCTURES

F. Stochino, S. Tattoni,

Università di Cagliari - DICAAR
Via Marengo, 2 – 09123 Cagliari, Italy

Abstract

The paper deals with the flexural failure of Reinforced Concrete elements under blast loads. The main topics and results of a PhD thesis are here summarized, whose aim was to develop theoretical dynamic and energy models capable of evaluating the dynamic response of R.C. elements under explosive load.

In the original work, models with different levels of complexity were presented, but for sake of simplicity only the simplest Single Degree Of Freedom (SDOF) system has been here discussed. Strain-rate effects are also accounted for.

A sensitivity analysis to determine the key parameters in beam response under blast load has been developed by means of the SDOF model. Results of numerical simulations obtained in terms of deflection and velocity have been fitted by proper polynomial least-square interpolation.

Among the various interpolations considering several parameters (peak load, positive phase duration, slenderness, span length, concrete strength, reinforcement ratio etc.) slenderness (corresponding to stiffness) and peak load prove to be the most important parameters, but span length (corresponding to mass) is also a key parameter. Other variables such as concrete strength and reinforcement ratio do not seem to have a high correlation with results.

Lastly some suggestions for blast-resistant bridge design are presented.

1 INTRODUCTION

Nowadays, the issue of structural safety under blast loading has become a dramatic problem. The tragic news of the terrorist attacks of recent years (9/11/2001, New York; 7/7/2005, London; 7/23/2005, Sharm El Sheik; 1/24/2011, Moscow; etc), raise important, urgent questions regarding the real safety and reliability of our buildings. Extreme loads such as impacts, explosions, etc., can occur in everyday life with unexpectedly high frequency. Actually, the problem of terrorist attacks, so important for strategic (Fig. 1) and military building design, has been linked to residential and industrial building explosion accidents.

Fig. 1: Explosion on a highway bridge in China caused by a truck carrying fireworks.

It is intuitively true that the effects of explosions on structures can be tremendously dangerous, since they can cause severe damage to buildings and, consequently, loss of lives. Since loads due to blast overpressure can be very extreme, structural elements should be endowed with enough strength and, above all, ductility to resist such loads.

The evaluation of building response under blast load is a very complex subject due to the great non-linearity of the phenomena involved. Both load and structural models are affected by several uncertainties, which increase along with increasing complexity of analysis and the number of parameters considered. In introducing this issue, it is important to define ‘‘explosion’’, as stated by Genova-Silvestrini [7]: “The term explosion indicates a violent reaction, typical of explosives, characterized by great development of gas and heat and consequent increase in the volume of reaction products". It is thus understandable that facing this type of problem involves different fields of physical science, chemistry and, of course, engineering. In particular, evaluating and predicting the time-history of blast-load pressure is a vast and interesting topic, but is not the real objective of this work. On the contrary, the structural collapse caused by a blast load is the main subject of this paper. Actually, in the case of explosion loads, the failure mechanism can be distinguished as a local or global one, as stated by De Matteis et alt. [8]:

- local failure of structural elements directly due to the effect of the wave impact on structural elements;
- global collapse affecting the whole structure: it often occurs following localized collapse and is closely related to structural robustness.

Obviously, global collapse is more dangerous. One of the characteristics required by modern performance-based codes is the capability to redistribute loads as a result of the collapse of a localized structural element. In design procedures, both types of collapse should be taken into consideration. In this work, the Authors investigate the resistance of flexural elements under blast load, focusing only on local failure.

2 BLAST LOADS

The explosion load model must take into account many variables which are difficult to determine a priori. A typical pressure time-history is shown in Fig. 2 (a) in case of detonation (wave velocity exceeds the speed of sound) and in Fig. 2 (b) in case of deflagration (wave velocity does not exceed the speed of sound). In the former case, the blockage ratio is not relevant, and the magnitude of the charge and its distance from the target become predominant. On the contrary, referring to deflagration, the blockage ratio plays a fundamental role, as does charge magnitude.

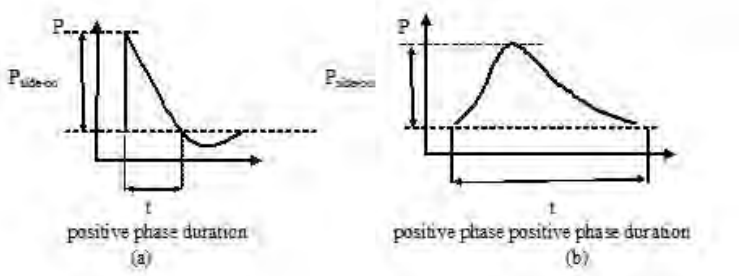

Fig. 2: Pressure time-histories for detonation (a) and deflagration (b).

In [9], the author proposes an overview of methods for assessing the effect of explosive action on buildings. He assumes to distinguish three categories:

- empirical methods: essentially statistical correlations of experimental data;
- semi-empirical methods: models based on simplified physical phenomenon;
- numerical methods: numerical solutions of the fluid dynamics equations governing the phenomenon (Computational Fluid Dynamics (CFD)).

Choosing the best method depends on how much information is given for the load scenario. In fact, the more sophisticated the model, the more parameters must be known.

Empirical models are simpler and generally less accurate. There are several manuals ([10] for example) which present graphs and tables showing the results of

various experimental analyses. These data can be very useful in initial assessment. They easily provide an order of magnitude of the variables involved and, within the limits of the experimental conditions in which they were obtained, are precise.

Semi-empirical models are developed by trying to interpret physical phenomenon assuming simplified hypothesis. There are several publications using this type of formulation (e.g.[11]. [12]). An interesting example is Hudson's method of evaluating the effect of compensation undergone by the pressure wave when it strikes a surface of finite width. In fact, the presence of edge effects produces a considerable pressure reduction on the target. Hudson in [13] proposes a series of assumptions (e.g. the pressure wave assumed to be plane) permitting a closed-form solution of the equations defining the problem. This method was recently rediscovered by Tyas et alt. [14], [15]. By means of experimental tests, the authors demonstrated that the real accuracy of this approach is greater than that obtained using the usual methods (e.g. ConWep software, etc.).

More complex models are developed by means of computational fluid-dynamic (CFD) solutions. Firstly, equations analytically representing the problem are assumed: the continuity equation, Navier Stokes' equation, the energy conservation equation. Actually, the main difficulty lies in the fact that these equations contain non-linear terms, and it is not always possible to find a solution in closed form. In most cases, it is necessary to resort to numerical discretization in space and time. The way in which the discretization (mesh) is done characterizes the calculation code and its numerical techniques. From the Lagrangian point of view, the evolutionary state of each particle is considered with a mesh which deforms and moves with the material. On the other hand, in the case of an Eulerian approach, the focus is on the state of the fluid at specific points in space at different instants in time. In this case, the mesh is fixed and is crossed by the moving material. Finally, there are codes using both systems according to varying situations (Arbitrary, Lagrangian, Eulerian, e.g.).

Explosive	Mass specific energy Q_x (k]/kg)	TNT equivalent (Q_x/Q_{TNT})
Nitroglycerin (liquid)	6700	1.481
C4 (91% RDX)	–	1.19–1.37
HMX	5680	1.256
Semtex	5660	1.250
RDX (cyclonite)	5360	1.185
Compound B (60% RDX 40% TNT)	5190	1.148
TNT	4520	1.000
Blasting gelatin	4520	1.000
ANFO (94% ammonium nitrate, 6% fuel oil) [6]	3932	0.870
60% nitroglycerin dynamite	2710	0.600

Table 1 Conversion factors for explosives.

As regards the problem of external explosions caused by terrorist attacks or accidents, the uncertainties and difficulties can be described at different levels of detail. Firstly, it is necessary to define the quantification of the explosive threat in

terms of kg of equivalent TNT. The equivalence factor is derived on the basis of energy considerations between TNT and other explosives, as shown in Table 1 for most common explosives.

The second level of uncertainty concerns the geometry scenario. It is usually defined by the distance between the position of the charge and the target structure and the relative position of the various objects on the scene (protective walls, street furniture, but also size and blockage ratio of the environment). The most common parameter generally used to describe this problem is stand-off distance d, the distance between the position of the charge and the target. In the current literature ([6], [7], [10]), these two variables (stand-off distance d and mass of TNT equivalent M) are expressed by means of a new quantity called scaled distance, as in Eq (1). The blast load time-history is often expressed as a function of time and stand-off distance.

$$z = \frac{d}{M^{1/3}} \quad (1)$$

For practical purposes it is possible to create an idealized pressure–time curve for a free-air explosion (Fig. 3) with the TNT equivalent charge weight M and standoff distance z.

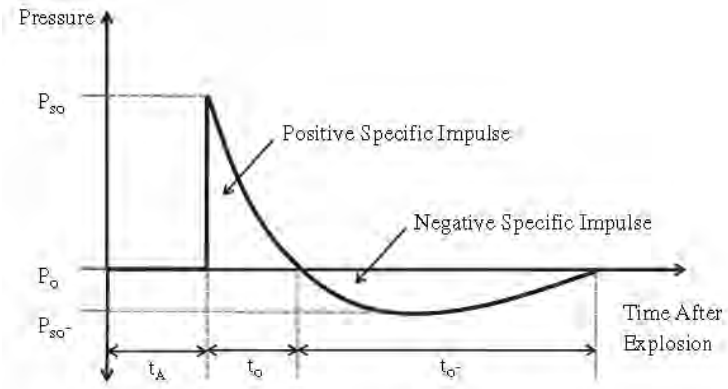

Fig. 3 Idealized pressure–time curve for free-air explosion (Department of the Army, 1990).

A hemispherical burst on a perfect reflecting surface will double the effective charge weight, while a reflection factor of 1.8 is more realistic when significant ground cratering is present. Commonly used “standard” airblast curves, often referred to as “spaghetti charts,” exist to predict the parameters required to define an idealized blast wave (Fig. 4).

The transmission of a shock front through a fluid (i.e., air) is a nonlinear process, and the interaction of a blast wave with a structure is a complex problem leading to significantly magnified pressures and impulses. Fig. 5 illustrates a blast wave reflecting off a structure. The magnification of the reflected pressure and impulse will vary depending on the magnitude of the peak incident overpressure and the orientation and location of the structure relative to the explosion source.

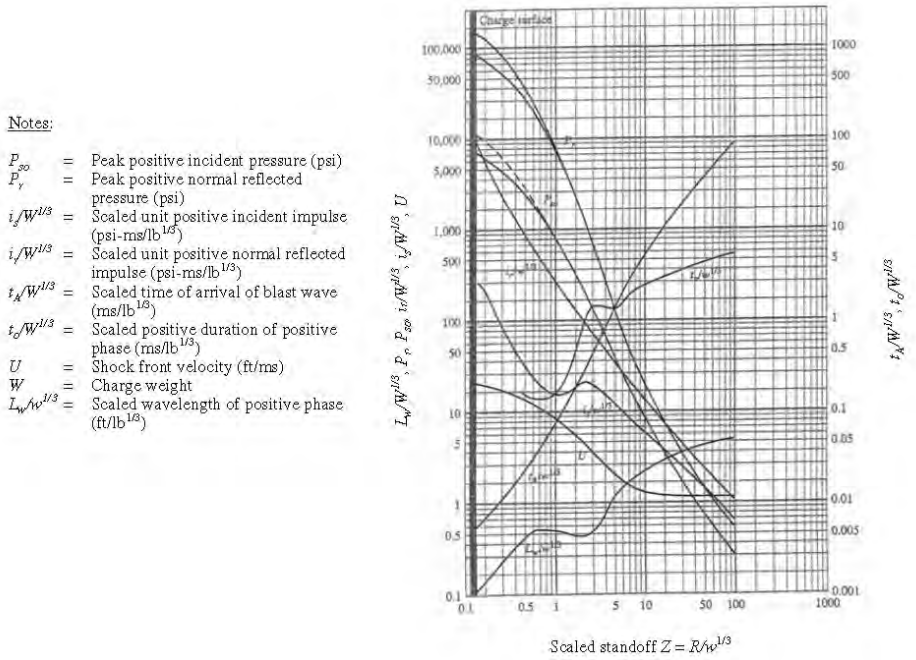

Fig. 4. Positive phase airblast parameters for hemispherical surface TNT detonation at sea level (Department of the Army, 1990).

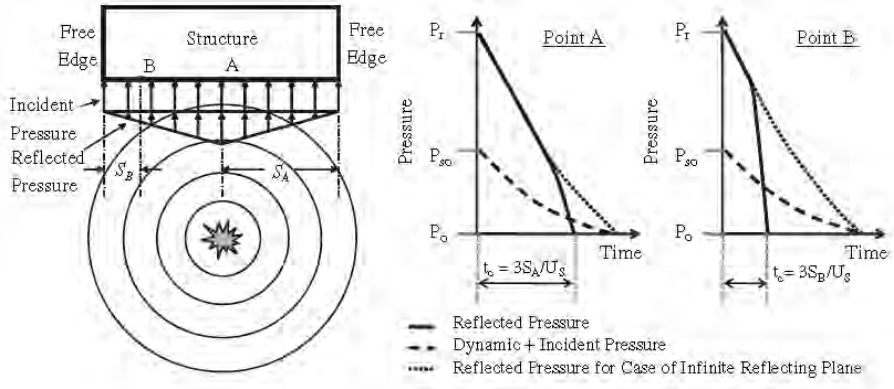

Fig. 5. Blast wave reflecting off structure (U.S. Army Engineer Research and Development Center, 2003).

Pressure peaks can be magnified by corners and confinement. For example, explosions located beneath a bridge deck will cause large uplift forces, and pressure build-up between girders and near the abutments can greatly amplify the applied load (Fig. 6).

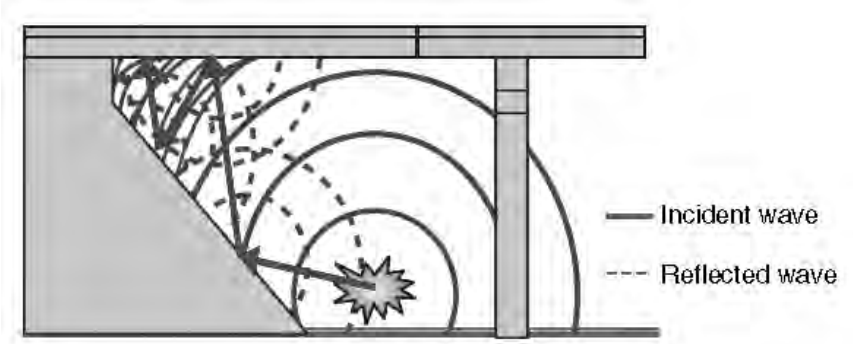

Fig. 6. Blast-wave propagation during below-deck explosion (Winget et al., 2005).

The present paper deals with the flexural failure of Reinforced Concrete elements (beams) under blast loads.

3 DYNAMIC RESPONSE TO BLAST LOADS

Determining the dynamic response of a reinforced concrete element under blast loads is not an easy task, in part due to the complexity of modelling the structural element (considering that the behaviour of the element under such loads is generally nonlinear and that properties of the materials are functions of the strain rate) and in part due to the difficulty of precisely defining the time variation and space distribution of the load. Actually, various simplified methods have been proposed to date. It is possible to identify three main theoretical approaches (see [16]) to the problem of a beam under blast load:

- rigid-plastic models;
- elastic-plastic Single Degree of Freedom models;
- modal approximation and distributed models.

3.1 Model evolution

The most elementary, common dynamic approach to model beams under blast load consists of schematizing the beam with a Single Degree of Freedom (SDOF) system. This approach simplifies both the theoretical formulation of the problem and calculations, but it usually requires the introduction of empirical formulas and, in addition, it does not provide full information on beam response. Actually, it only provides the fundamental response mode normally responsible for overall structural failure [16].

Colin Morison distinguishes two main SDOF approaches:

- Modal Method.
- Equivalent SDOF Method

The modal method was first presented in 1946 in the US Manual, ‘‘Fundamentals

of Protective Design (Non-Nuclear)'' EM 1110-345-405, re-issued in 1965 as TM5-855-1 [17]. This method assumes that the elastic forced response of the real element will be approximated by its first mode of free vibration. In case of elastic-pure plastic resistance function, the equation of motion can be solved in a close form, and referring to an idealized blast load, with triangular/rectangular time-history, maximum deflection can easily be calculated in order to develop a diagram like the one depicted in Fig. 7

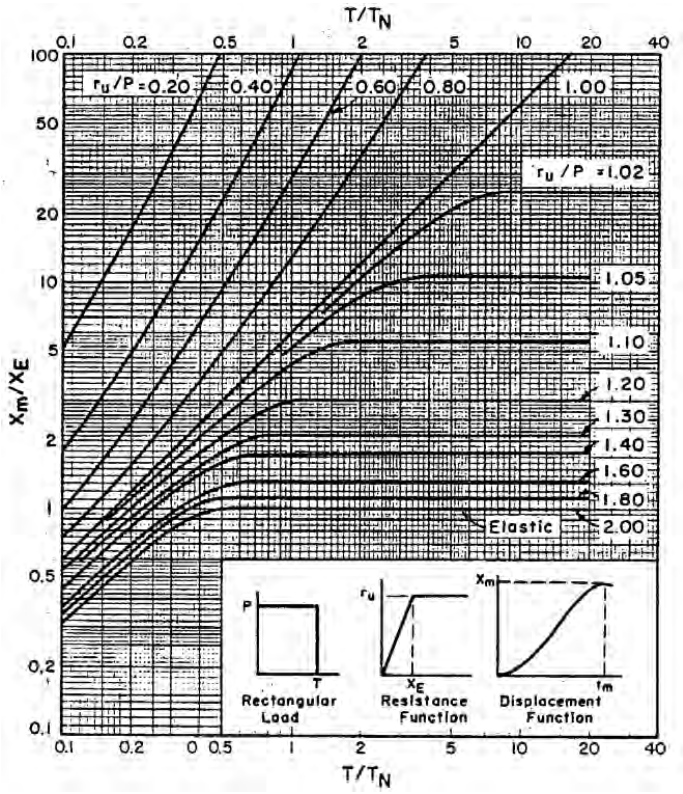

Fig. 7: Chart to calculate maximum deflection response X_m (from [10] fig. 3.56) attained at time t_m. The blast load is defined by its duration T and peak value P. The SDOF elastic deflection is X_E and r_u is its ultimate resistance, finally its natural period is T_N.

In the fifties, knowledge in this field increased, and the elastic-plastic model was considered. In an early work, Seiler et al. [18] modelled, by means of SDOF, a simply-supported beam under impulsive loading. They assumed that the initial velocity was a half sine wave. In this case, a simple mass-spring system can model the behaviour of elastic-plastic and rigid-plastic beams in order to develop a comparison between the two approaches. Then Brooks and Newmark, in [19], investigated numerous dynamic structural problems. In particular, Newmark [20]-[21] was an influential proponent of the modal method, having calculated several modal period formulas and corresponding stiffness and strength expressions.

According to Morison, this method presents two drawbacks:

- a lack of versatility due to the fact that charts and diagrams based on it were developed only for some specific load time-histories;.
- inadequate treatment of reaction forces. This method considers only forcing function distributed spatially with the same shape as the vibration shape, and this leads to underestimation of the reaction at member supports. In addition, this problem precludes suitable dynamic shear design for reinforced concrete members.

The equivalent SDOF method appeared in 1957 in the US Army Corps of Engineers manual "Design of structures to resist the effects of atomic weapons". This method relies on calculation of SDOF parameters based on the equivalence of energy: the equivalent mass must have equal kinetic energy, the equivalent resistance must have equal internal strain energy and the equivalent loading must have equal external work to the real distributed element. These equivalent factors can be calculated for different structures with different boundary and loading conditions. In Fig. 8, some examples are shown of the value of the load factor K_L, mass factor K_M and other parameters of the equivalent SDOF for simply-supported beams.

In the last fifty years, several versions of this method were developed, and it is frequently used nowadays as well.

Loading diagram	Mass diagram	Strain range	Load factor, K_L	Mass factor, K_M	Load–mass factor, K_{LM}	Maximum resistance, R_m	Stiffness, k	Support shear, V_s	Ultimate shear stress, v	Dynamic reaction, V
Uniformly distributed load $F = pL$	Uniformly distributed mass $M = mL$	Elastic	0.64	0.50	0.78	$\frac{8M_p}{L}$	$\frac{384EI}{5L^3}$	$\frac{R_m}{2}$	$R_m\left(\frac{1}{2d_c}-\frac{1}{L}\right)$	$0.39R + 0.11F$
		Plastic	0.50	0.33	0.66	$\frac{8M_p}{L}$	0			$0.38R_m + 0.12F$
	Central point mass M	Elastic	0.64	1.0	1.56	$\frac{8M_p}{L}$	$\frac{384EI}{5L^3}$	$\frac{R_m}{2}$	$R_m\left(\frac{1}{2d_c}-\frac{1}{L}\right)$	$0.50R$
		Plastic	0.50	1.0	2.0	$\frac{8M_p}{L}$	0			$0.50R_m$
Central point load F	Uniformly distributed mass $M = mL$	Elastic	1.0	0.49	0.49	$\frac{4M_p}{L}$	$\frac{48EI}{L^3}$	$\frac{R_m}{2}$	$\frac{R_m}{2d_c}$	$0.78R - 0.28F$
		Plastic	1.0	0.33	0.33	$\frac{4M_p}{L}$	0			$0.75R_m - 0.25F$
	Central point mass M	Elastic	1.0	1.0	1.0	$\frac{4M_p}{L}$	$\frac{48EI}{L^3}$	$\frac{R_m}{2}$	$\frac{R_m}{2d_c}$	$0.50R$
		Plastic	1.0	1.0	1.0	$\frac{4M_p}{L}$	0			$0.50R_m$

Fig. 8: Equivalent SDOF factors for simply-supported beams (from [6] table A1).

3.2 Characteristics of a SDOF model

Now we will assess the dynamic response of a beam by means of a single degree of freedom (SDOF) model. In Fig. 9a, a real beam is depicted (which, as an example, is

supposed to be simply supported and subjected to a uniformly-distributed load), while its equivalent SDOF system is sketched in Fig. 9b. It should be noted that damping is disregarded, since successive loading cycles are not considered; in fact, the first peak displacement is the most severe condition, as it is unlikely the structure will collapse after unloading**Errore. L'origine riferimento non è stata trovata.**.

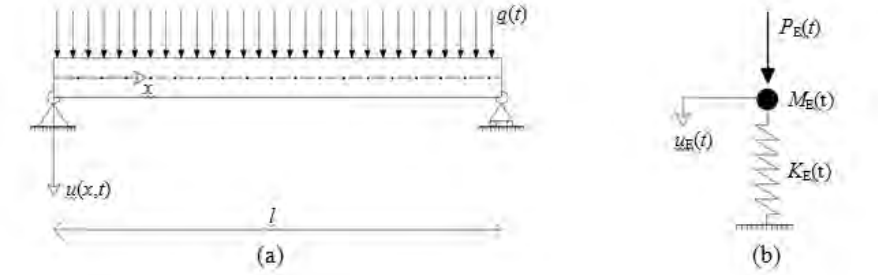

Fig. 9: (a) Real beam; (b) equivalent SDOF model of the real beam.

The elastic-plastic behaviour of the SDOF system can be represented by a bilinear load-displacement diagram, as shown in Fig. 10b. The latter can be derived from the bending moment-curvature diagram of the beam as described in the following

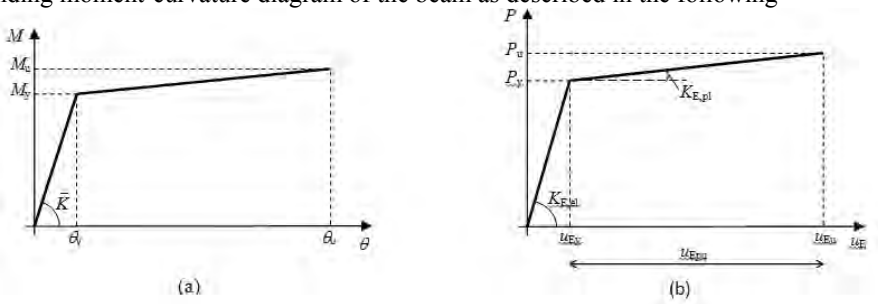

Fig. 10: (a) Bilinear bending moment-curvature diagram of the beam; (b) corresponding bilinear load-displacement diagram of the equivalent SDOF model.

Yield load Py is easily determined from the yield bending moment My by means of equilibrium considerations:

$$M_y = \frac{q_y \cdot l^2}{8} \quad \Rightarrow \quad P_y = q_y \cdot l = \frac{8 \cdot M_y}{l} \tag{2}$$

where q_y is the uniformly-distributed load acting on the beam in the yield state. Yield displacement u_{Ey} can be calculated using the well-known formula provided by the linear elastic theory of beams:

$$u_{Ey} = \frac{5 \cdot q_y \cdot l^4}{384 \cdot \bar{K}} = \frac{5 \cdot P_y \cdot l^3}{384 \cdot \bar{K}} \tag{3}$$

where $\bar{K} = M_y / \theta_y$ is the elastic bending rigidity of the beam (see Fig. 10a). Hence, the elastic stiffness of the SDOF system is given by:

$$K_{\mathrm{E,el}} = \frac{P_{\mathrm{y}}}{v_{\mathrm{Ey}}} = \frac{384 \cdot \bar{K}}{5 \cdot l^3} \tag{4}$$

The ultimate load P_{u} can again be obtained from equilibrium conditions:

$$M_{\mathrm{u}} = \frac{q_{\mathrm{u}} \cdot l^2}{8} \quad \Rightarrow \quad P_{\mathrm{u}} = q_{\mathrm{u}} \cdot l = \frac{8 \cdot M_{\mathrm{u}}}{l} \tag{5}$$

where q_{u} is the uniformly-distributed load on the beam at the ultimate state. Ultimate displacement u_{Eu} is evaluated by assuming that a concentrated plastic hinge is formed at the mid-span section of the beam, as shown in Fig. 11a. Here, φ_{p} indicates the plastic rotation at any time after generation of the plastic hinge, while u_{Ep} represents the corresponding plastic displacement at the mid-span section. At the ultimate state $\varphi_{\mathrm{p}} = \varphi_{\mathrm{pu}}$, hence total plastic displacement, $u_{\mathrm{Ep}} = u_{\mathrm{Epu}}$ can be calculated as:

$$u_{\mathrm{Epu}} = \frac{\varphi_{\mathrm{pu}}}{2} \cdot \frac{l}{2}. \tag{6}$$

By introducing plastic hinge length l_{p} (see Fig. 11b) and by denoting total plastic curvature by θ_{p} ($\theta_{\mathrm{p}} = \theta_{\mathrm{u}} - \theta_{\mathrm{y}}$), assumed to be constant over l_{p}, the ultimate displacement u_{Eu} can finally be derived:

$$u_{\mathrm{Eu}} = u_{\mathrm{Ey}} + u_{\mathrm{Epu}} = u_{\mathrm{Ey}} + \frac{\varphi_{\mathrm{pu}}}{2} \cdot \frac{l}{2} = u_{\mathrm{Ey}} + \frac{\theta_{\mathrm{p}} \cdot l_{\mathrm{p}}}{2} \cdot \frac{l}{2} = u_{\mathrm{Ey}} + \frac{1}{4} \cdot \left(\theta_{\mathrm{u}} - \theta_{\mathrm{y}}\right) \cdot l_{\mathrm{p}} \cdot l. \tag{7}$$

Finally, plastic stiffness of the SDOF system is given by:

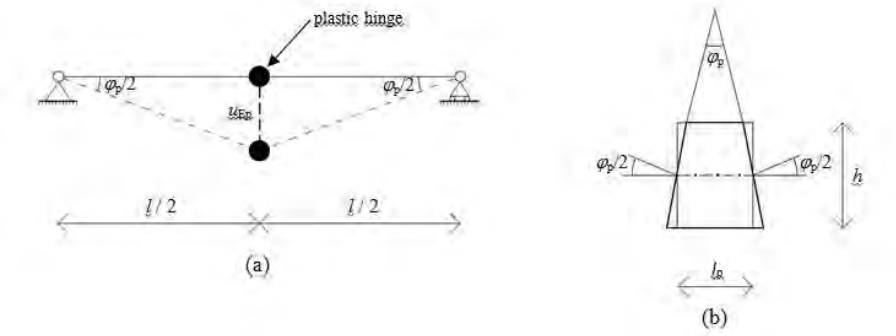

Fig. 11: (a) Plastic deflections of the beam with a concentrated plastic hinge at the mid-span section; (b) schematic representation of the plastic hinge.

Finally, plastic stiffness of the SDOF system is given by:

$$K_{\mathrm{E,pl}} = \frac{P_{\mathrm{u}} - P_{\mathrm{y}}}{u_{\mathrm{Eu}} - u_{\mathrm{Ey}}}. \tag{8}$$

The main drawback of this approach is that plastic hinge length l_{p} cannot be

determined *a priori*. Many approximate expressions for l_p are available in the literature. Here, the simple formula provided by Mattock is adopted:

$$l_p = d + 0.05 \cdot l \,. \tag{9}$$

For the sake of clarity it is important to point out that the effective height d is defined in Fig. 12.

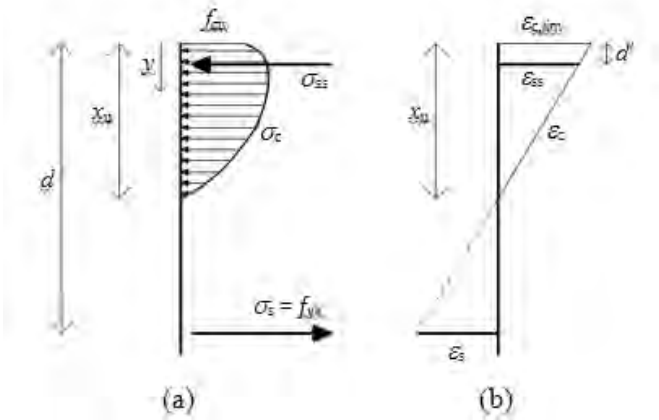

Fig. 12: (a) Stress distribution over the cross-section at the ultimate state; (b) strain diagram at the ultimate state.

3.3 Motion equations of the SDOF system

Motion in the SDOF system under an external dynamic force P_E is described by the following set of ordinary differential equations (refer to Fig. 9b and Fig. 10b):

$$M_{E,el}\frac{d^2u_E(t)}{dt^2} + K_{E,el}(t)u_E(t) = P_E(t) \quad \text{for } 0 \le u_E \le u_{Ey} \qquad a);$$
$$M_{E,pl}\frac{d^2u_E(t)}{dt^2} + K_{E,pl}(t)u_E(t) + \left(K_{E,el}(t) - K_{E,pl}(t)\right)u_{Ey} = P_E(t) \quad \text{for } u_{Ey} < u_E \le u_{Eu} \qquad b). \tag{10}$$

It is important to observe that elastic and plastic stiffness ($K_{E,el}$ and $K_{E,pl}$) depends on time t, since it is updated at each step of the calculation due to strain rate effects, as explained in following section.

The equivalent load P_E is simply given by $P_E = q \cdot l$. The elastic and plastic equivalent masses ($M_{E,el}$ and $M_{E,pl}$) are obtained by multiplying the total mass of the beam (M_b) by a "load-mass factor", depending both on the type of regime (either elastic or plastic) and on the beam supports and loads; in particular, for a simply-supported beam with a uniformly distributed load, $M_{E,el} = 0.78 \cdot M_b$ and $M_{E,pl} = 0.66 \cdot M_b$.

3.4 Strain-rate effects for the SDOF system

The effects of strain rate are also taken into account for the equivalent SDOF model. Since the dynamic properties of the materials are given in terms of their strain rates (see Fig. 13 and Fig. 14**Fig. 14**), it is necessary to relate the SDOF system to the

associated (real) beam, from which the strain rates of concrete and steel can be assessed.

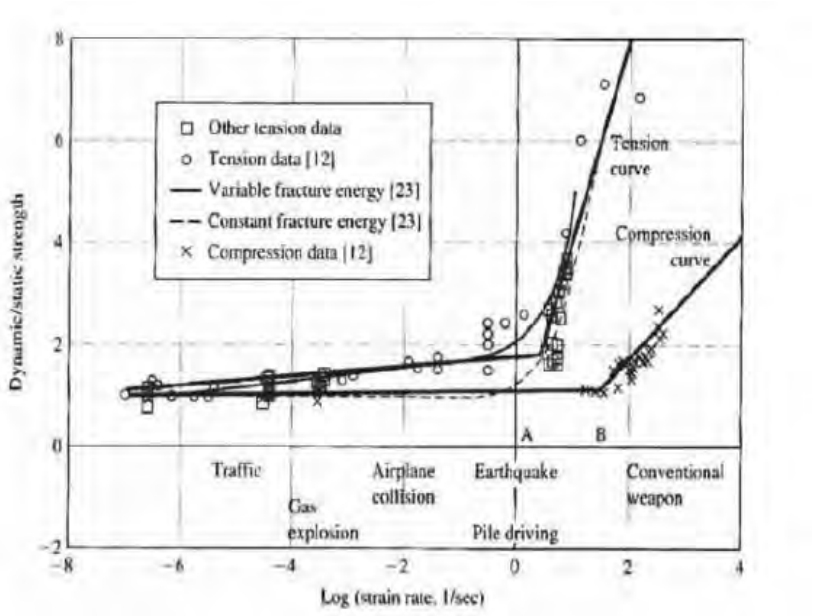

Fig. 13: Concrete strain-rate effects on strength (Tedesco 1999).

Once the equivalent displacement u_E and equivalent velocity $\dot{u}_E = \mathrm{d}u_E / \mathrm{d}t$ are calculated at each time step by solving either Eq. (10) or Eq. (10), the curvature θ_E and the curvature rate $\dot{\theta}_E = \mathrm{d}\theta_E / \mathrm{d}t$ at the mid-span section of the associated beam can be evaluated. In the elastic regime, θ_E and $\dot{\theta}_E$ are obtained from linear elastic theory; in particular, for a simply-supported beam with a uniformly distributed load, they are given by:

$$\theta_E = \frac{48 \cdot u_E}{5 \cdot l^2} \quad \text{for } 0 \le u_E \le u_{Ey} \quad a);$$
$$\dot{\theta}_E = \frac{48 \cdot \dot{u}_E}{5 \cdot l^2} \quad \text{for } 0 \le u_E \le u_{Ey} \quad b). \qquad (11)$$

In the plastic regime, on the other hand, it is supposed that a concentrated plastic hinge is generated at the mid-span section of the associated beam, as shown in Fig. 11a. Accordingly, in this case θ_E and $\dot{\theta}_E$ can be evaluated by means of the following expressions:

$$\theta_E = \theta_y + \frac{\varphi_p}{l_p} = \theta_y + 2 \cdot \frac{u_{Ep}}{l/2} \cdot \frac{1}{l_p} = \theta_y + 2 \cdot \frac{u_E - u_{Ey}}{l/2} \cdot \frac{1}{l_p} \quad \text{for } u_{Ey} \le u_E \le u_{Eu} \quad a); \qquad (12)$$

$$\dot{\theta}_{\mathrm{E}} = 2 \cdot \frac{\dot{u}_{\mathrm{E}}}{l/2} \cdot \frac{1}{l_{\mathrm{p}}} \quad \text{for } u_{\mathrm{Ey}} \le u_{\mathrm{E}} \le u_{\mathrm{Eu}} \qquad b) \,.$$

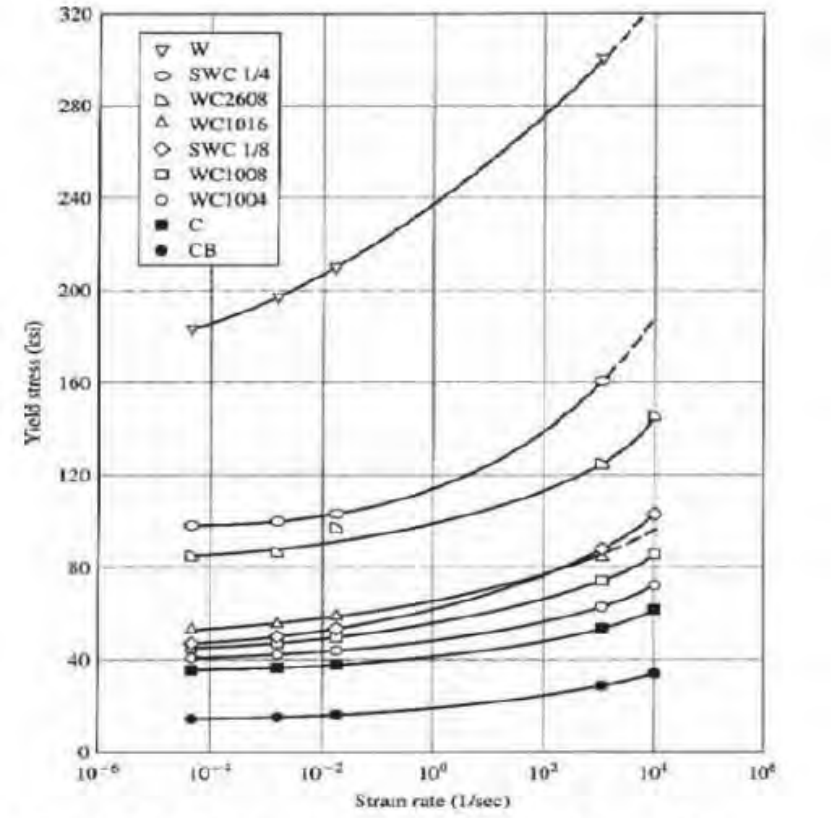

Fig. 14: Effects of strain-rate on yeld sterss for various metals (Tedesco 1999).

At each step of the calculation, the value of θ_{E} (given by either Eq. (**11**) or Eq. (**12**)) allows to determine the value of the bending moment M from the bending moment-curvature diagram in Fig. 10a. Then, by imposing rotational equilibrium regarding tensile reinforcement, the neutral axis depth (here denoted as $\bar{x}$) can easily be evaluated. Finally, the strain rates of concrete and of tensile and compressive steel reinforcements are calculated using the following formulas:

$$\begin{aligned} \dot{\varepsilon}_{\mathrm{c}} &= \dot{\theta}_{\mathrm{E}} \cdot \bar{x} \qquad a) \,; \\ \dot{\varepsilon}_{\mathrm{s}} &= \dot{\theta}_{\mathrm{E}} \cdot (d - \bar{x}) \qquad b) \,; \end{aligned} \tag{13}$$

$$\dot{\varepsilon}_{ss} = \dot{\theta}_E \cdot (\bar{x} - d') \qquad c) .$$

The absolute values of the strain rates given by Eqs. (13) are introduced into specific equations to update the properties of the materials.

4 EQUATIONS IMPLEMENTATION

The random nature of the explosion load, associated with the random nature of material properties and geometric dimensional characteristics, implies the need to consider them in the analysis in order to have a more correct estimation of structural behaviour. Therefore, when the randomness of these parameters is taken into consideration, the response of the structure assumes a probabilistic nature, making it necessary to look into the reliability measure. The probabilistic approach to structural reliability in the case of a blast load is a current topic in structural engineering.

In order to face such a complex problem, it is essential to determine the key parameters in blast load response. For this reason, a sensitivity analysis was developed [2]. Numerical simulations by means of the previous SDOF model have been developed, considering different load scenarios and beam geometrical and strength characteristics. In this way, it is possible to search for any correlations between the response of the SDOF in terms of displacement/velocity and the different parameters defining the dynamic problem: peak load, slenderness, span length, etc.

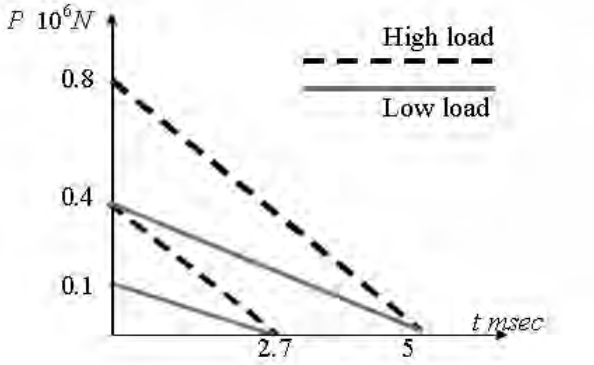

Fig. 15. Time-histories of the two load conditions: low and high.

Somewhere about 4000 runs of the SDOF model were performed, 2000 under high load and 2000 under low load (Fig. 15). For the sake of clarity it is important to remember that the collapse criterion corresponds to the attainment of the ultimate concrete strain. In the case of high load and slenderness greater than 12, the percentage of failures reaches 50%; on the contrary, in case of low load and lower slenderness, almost all beams resist the blast load (Fig. 16).

These results are important because they underline the role of an important parameter: slenderness of the beam defined as the ratio between span length and the effective height of the cross-section. Correlation between structural reliability and

slenderness is possible, and it is obviously linked to the fact that in the case of flexural models, beam stiffness is strictly dependent on the latter parameter.

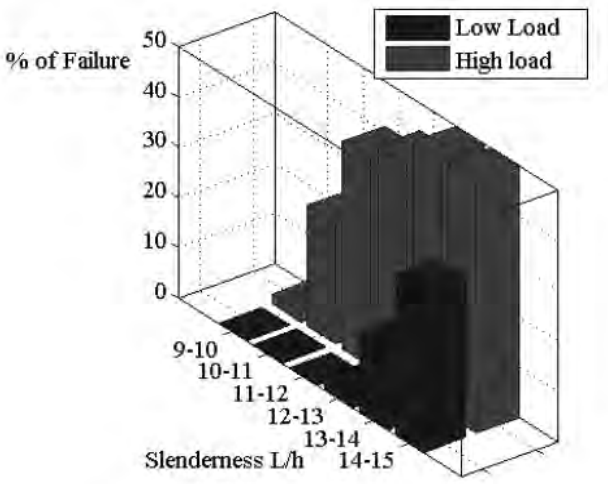

Fig. 16. Collapse percentage of the beams examined with reference to both load scenarios.

Fitting functions were obtained with a sufficiently-high number of simulations [23]. They would correspond to the most probable response of the given beam under a given blast load. In order to have an idea of the useful development of this analysis Table 2 and Table 3 have been prepared. Referring to High Load (peak load $0.4\text{-}0.8\times10^6$ N in Table 2) and Low load conditions (peak load $0.1\text{-}0.4\times10^6$ N in Table 3) the most probable maximum displacements of a beam under the assumed hypothesis[1] are expressed.

Slenderness\Peak Load	$4\cdot10^5$ N	$5\cdot10^5$ N	$6\cdot10^5$ N	$7\cdot10^5$ N	$8\cdot10^5$ N
9	0.044	0.061	0.079	0.097	0.114
10	0.079	0.096	0.114	0.131	0.149
11	0.114	0.131	0.149	0.166	0.184
12	0.149	0.166	0.184	0.201	0.219
13	0.184	0.201	0.219	0.236	0.254
14	0.218	0.236	0.254	0.271	0.289
15	0.253	0.271	0.288	0.306	0.324

Table 2 : High Load – Maximum Displacement estimation (in meter) based on the poly 1-1 model Slenderness/Peak Load

It is important to point out that, due to the limited number of numerical experiments (4000 runs of the SDOF model), only the linear polynomial function of slenderness and peak load has been considered to prepare these tables. Actually, the limited number of the required parameters for a linear function and the significance of slenderness and peak load variables lead to this choice. In fact, more complex

[1] Simple supported, uniformly distributed load with triangular time history etc.

polynomial relationships with more coefficients would have required a larger number of numerical experiments to become significant.

Hence, referring to Table 2 it is interesting to underline that the black thick line identifies the conditions in which the probability of collapse (attainment of the ultimate concrete strain) approaches and exceeds 50% in case of high load. This threshold of safety is never reached in case of low load.

In conclusion, a systematic application of the methodology presented in this chapter could produce several useful tables like these two (Table 2 and Table 3). In this way a designer may quickly know what are the maximum displacement, the maximum velocity and the reliability measures (in terms of collapse probability) of a given type of beam under a given condition of the load.

Slenderness\Peak Load	$1 \cdot 10^5$ N	$1.5 \cdot 10^5$ N	$2 \cdot 10^5$ N	$3 \cdot 10^5$ N	$4 \cdot 10^5$ N
9	N.V.	0.005	0.017	0.042	0.066
10	0.011	0.023	0.036	0.060	0.085
11	0.030	0.042	0.054	0.079	0.104
12	0.048	0.061	0.073	0.098	0.123
13	0.067	0.080	0.092	0.117	0.141
14	0.086	0.098	0.111	0.135	0.160
15	0.105	0.117	0.129	0.154	0.179

Table 3 : Low Load – Maximum Displacement estimation (in meter) based on the poly 1-1 model Slenderness/Peak Load.

5 DESIGN STRATEGIES[2]

Methods that separate the calculation of blast-wave propagation effects from the determination of structural response are considered "uncoupled," and they typically provide conservative predictions of loads acting on structural components. Therefore they often provide conservative load values for designing structural members.

Unlike uncoupled analyses, coupled analysis methods consider blast-wave propagation and structural response together as they interact over time. Thus, a structure can vent pressure through localized failure, and the forces resulting in many members will be smaller and more realistic than those predicted by uncoupled analysis approaches[3].

A sketch of different calculation scenarios is shown in Fig. 17. It is worth to observe that because uncoupled analysis methods usually provide conservative blast propagation and structural response predictions, most design cases do not require the increased costs associated with coupled analysis methods.

There are several main differences between the designs of buildings and bridges to resist blast loads. In fact, a highway overpass is a bridge that crosses over another road or railway, and these structures commonly have extensive access below the deck and near columns via parking areas, traffic lanes, sidewalks, or other general unobstructed areas. Therefore, gaining access to structural members is much easier for bridges than buildings, creating the possibility of a design threat with a significantly smaller standoff distance. Structural elements such as bridge supports, columns and decks are

[2] Many items and figures in this paragraph are reported from [22]

[3] This is the design approach of Italian construction Code DM 14/01/2008 cap. 3.6.2.

directly exposed to blast waves. On the contrary, structural members in buildings, such as columns and beams, are usually behind a façade and are only indirectly loaded by a blast wave.

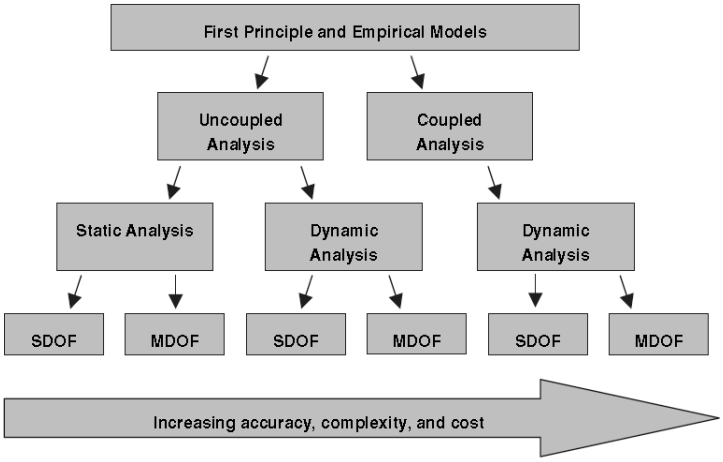

Fig. 17. Flowchart of possible analysis methods (Winget, 2003).

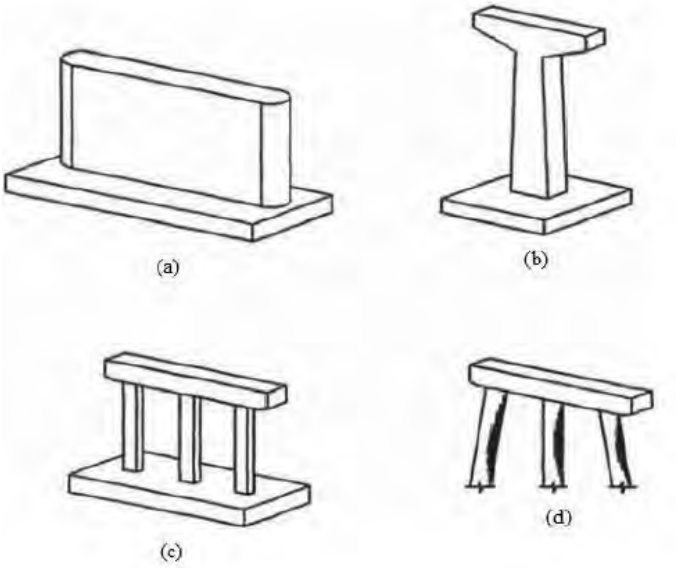

Fig. 18. Typical column types: a) solid, b) single column, c) multi-column, d) pile bent (NYSDOT, 2006).

Dealing with blast effects on bridge structures, the most considerable elements are supports (abutments, columns, piers). In Fig. 18 common types of columns are represented.

As suggested in, NCHRP report 645 for the purpose of designing substructure components for blast loads, the substructures shall be classified as Blast Design Category A, B or C based on the value of the scaled standoff Z as follows:

- • For Blast Design Category A: $Z > 3$
- • For Blast Design Category B: $3 \geq Z > 1.5$
- • For Blast Design Category C: $Z \leq 1.5$

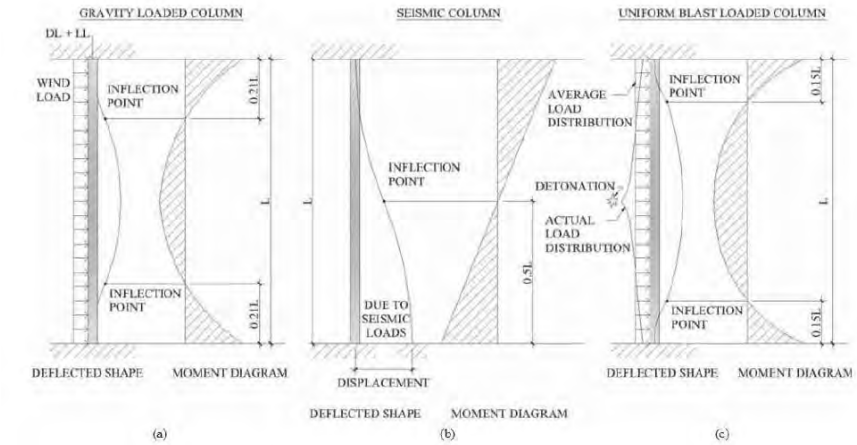

Fig. 19. Moment diagram and detected shape for each load case: a) typical, b) seismic, c) blast.

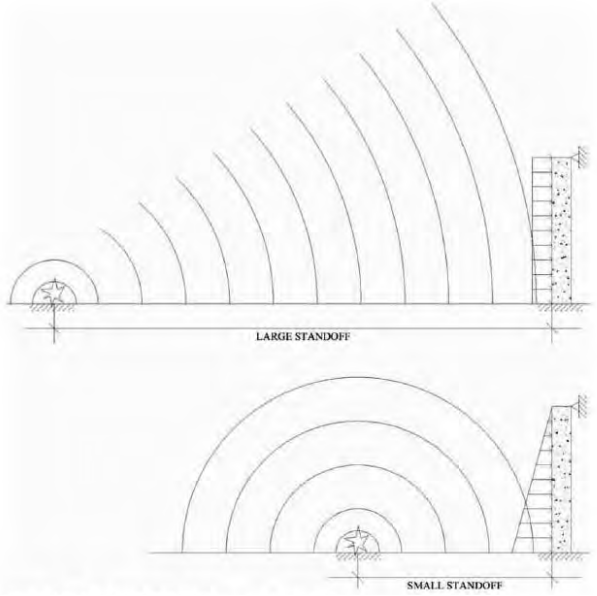

Fig. 20. Blast load distribution versus standoff.

The uncoupled approach by means of SDOF method begins from determination of peak value of pressure and his distribution. They depend on stand-off distance, as shown in Fig. 20. The equivalent Force-Displacement law (e.g as in Fig. 10) may be

calculated on the basis of a cinematic approach as shown in Fig. 21. The dynamic response is then evaluated as depicted in chapter 3.

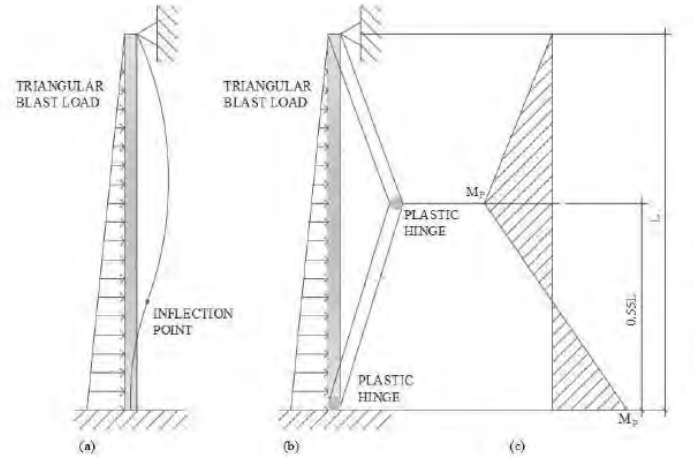

Fig. 21. Plastic hinge analysis for blast-loaded column: a) detected shape, b) plastic hinge locations, c) plastic moment.

It should be noted that differently from beams, ductility of section is strongly affected by axial force. Therefore more attention should be paid to reinforcement details in order to increase concrete confinement (Fig. 22 and Fig. 23).

Experimental observations show that increasing the volumetric reinforcement ratio is beneficial to the response of blast-loaded columns because it increases the column ductility and shear capacity. Direct shear is a major concern for blast-loaded columns, and adequate shear capacity is needed to ensure that columns fail in a ductile manner. Accordingly, to meet the high shear demands placed on a blast-loaded column in Category C, more stringent transverse reinforcement requirements than those used for seismic design are needed. Equation 14 is recommended as the minimum transverse reinforcement ratio for all circular blast-designed columns, while Equation 15 is recommended as the minimum area of transverse reinforcement for all rectangular blast-designed columns. Columns meeting these minimums tested at a small standoff sustained minor and extensive damage; however, the core still remained intact and the column could still carry load. Essentially, 50% more confinement is recommended for blast-designed columns over current seismic provisions to improve the ductility and energy dissipation capacity of the cross-section.

$$\rho_s \geq 0.18 \frac{f'_c}{f_y} \qquad (14)$$

$$A_{sh} \geq 0.18 s h_c \frac{f'_c}{f_y} \qquad (15)$$

where:
f'c = specified compressive strength of concrete at 28 days (psi)
fy = yield strength of reinforcing bars (psi)

s = vertical spacing of hoops, not exceeding 4 in. (in.)
hc = core dimension of column in the direction under consideration (in.)

This new minimum amount of transverse reinforcement should be applied over the entire column height to account for the uncertainty associated with potential blast locations.

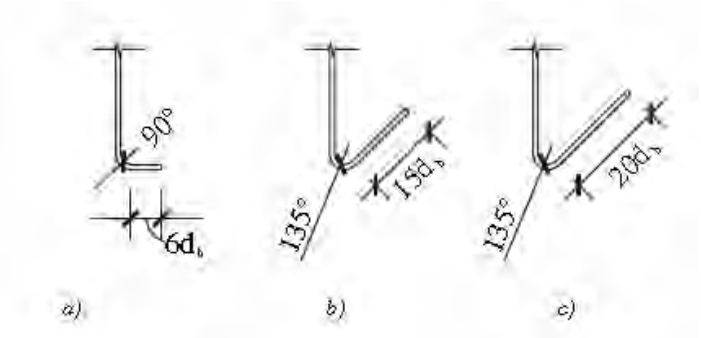

Fig. 22. Discrete tie anchorage: a) Design Category A, b) Design Category B, c) Design Category C..

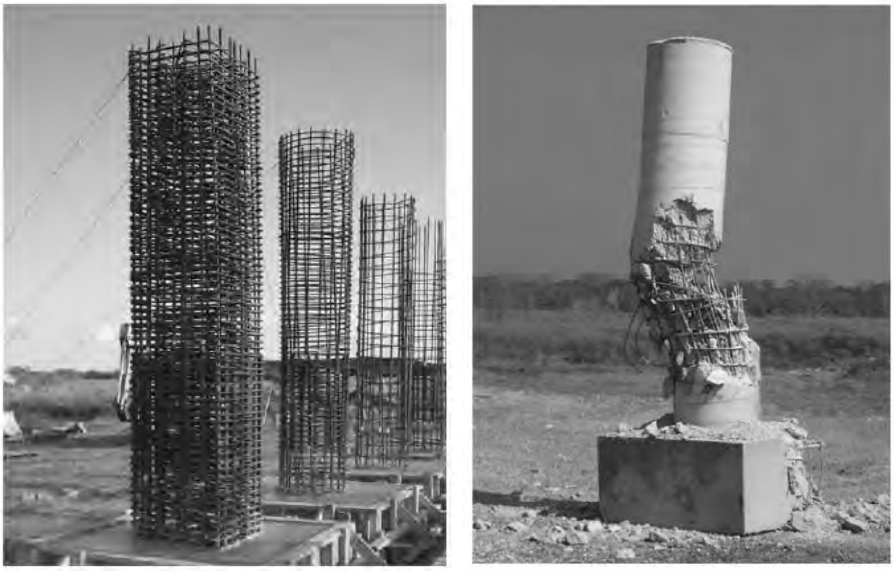

Fig. 23. Different steel cages and plastic hinge after blast.

6 REFERENCES

[1] Carta G, Stochino F. "Theoretical models to predict the flexural failure of reinforced concrete beams under blast loads". Engineering Structures, Volume 49, April 2013, Pages 306–315 (2013), dx.doi.org/10.1016/j.engstruct. 2012.11.008.

[2] Acito M. Stochino F. Tattoni S "Structural response and reliability analysis of rc beam subjected to explosive loading". International Conference: PROTECT 2011 "Protection & Strengthening of Structures under Extreme Loading" – Lugano 08/30 –09/01 2011 - Applied Mechanics and Materials Vol. 82 (2011) pp 434-439 doi:10.4028/www.scientific.net/AMM.82.434.

[3] Tattoni S–Stochino F.(2012): "Azioni esplosive sulle strutture in c.a." 19° Congresso CTE, Bologna 11/8-10 2012-Pag. 407-417, ISBN: 978-88-903647-9-2.

[4] Acito M. Stochino F. Tattoni S., "Analisi della sicurezza di travi in c.a. soggette ad azioni da esplosione". Giornate AICAP 2011 – Le prospettive di sviluppo delle opere in calcestruzzo strutturale nel terzo millennio, Padova 05/19-21 2011 – Pag. 3-11.

[5] Stochino F. Tattoni S., "Incremento prestazionale per edifici in c.a. resistenti ad esplosione e relativa valutazione economica". Giornate AICAP 2011 – Le prospettive di sviluppo delle opere in calcestruzzo strutturale nel terzo millennio, Padova 05/19-21 2011 – Pag. 375-380.

[6] G. C. Mays, P. D. Smith, (1995), "Blast Effect on Buildings"- second edition, Thomas Telford Publications, London ISBN: 978-0-7277-3521-8.

[7] B. Genova, M. Genova, M.Silvestrini, (2010), "Sicurezza degli edifici nei riguardi dei fenomeni esplosivi",UTET Scienze Tecniche, ISBN: 978-88-598-0415-4.

[8] G. De Matteis, E. Cadoni, D.Asprone, (2010), "Analysis of Behaviour of Construction Under Impact and Explosions: Approaches for Structural Analysis, from Material Modeling to Structural Response", Final Report of Urban Habitat Constructions under Catastrophic Events , edited by Mazzolani, Taylor & Francis Group, London ISBN: 978-0-415-60686-8, p. 161-178.

[9] A. M. Remennikov, "A Review of Methods for Predicting Bomb Blast Effects on Buildings", Journal of Battlefield Technology, 2003, 6(3), 5-10.

[10] TM 5-1300 (1990), Structures to Resist the Effects of Accidental Explosion, Departments of the Army, the Navy and the Air Force, TM 5-1300, NAVFAC P-379, AFR 88-22.

[11] C.N. Kingery and G.Bulmash, "Airblast Parameters from TNT Spherical Air Burst and Hemispherical Surface Burst", (1984), Report ARBL-TR-02555, U.S. Army BRL, Aberdeen Proving Ground, MD.

[12] US DEPARTMENT OF DEFENSE (DOD), "Unified Facilities Criteria UFCDOD: Structures to Resist the Effect of Accidental Explosions", (2008), UFC 3-340-02, Washington, D.C.

[13] C.C. Hudson,"Sound Pulse Approximations to Blast Loading (with comment on Transient Drag", Sandia Corporation Technical Memorandum (1955), SC-TM-191-55-51.

[14] A. Tyas, J.A. Warren, T. Bennet, S.D. Fay, "Prediction of Clearing Effects in Far-Field Blast Loading of Finite Targets", Shock Waves (2011), 21, pp 111-119 doi: 10.1007/s00193-011-0308-0.

[15] A. Tyas, T. Bennet, J.A. Warren, S.D. Fay, S. E. Rigby, "Clearing of Blast Waves on Finite Sized Targets- an Overlook Approach", Proceedings of Performance, Protection and Strengthening of Structures under extreme Loading, in Applied Mechanics and Materials Vol. 82 (2011), pp 669-674, doi:10.4028/www.scientific.net/AMM.82.669.

[16] Zhu F. & Lu G. A Review of Blast and Impact of Metallic and Sandwich Structures, Electronic J Struct Eng, 7 Special Issue: Loading on Structures (2007) , 92-101.

[17] Fundamentals of protective design (Non-nuclear) TM 5-855-1. Washington, DC: Department of the Army; March 1965. (Reprint of former document 1110-345-405, 1946).

[18] Seiler J.A., Cotter B.A., Symonds P.S., Providence R.I., Impulsive Loading of Elastic-Plastic Beams. J. Appl. Mech. (1956) 23, 515-521.

[19] Brooks N.B., Newmark N.M., The response of simple structures to dynamic loads, Technical report to ONR contract N6ori-071(06), Task Order VI Project NR-064-183 University of Illinois Urbana, Illinois, 1953.

[20] Newmark NM. An engineering approach to blast resistant design, American Society of Civil Engineers Transactions, Paper No. 2786, vol. 121, 1956. p. 45.

[21] Design of structures to resist Nuclear weapon effects. ASCE manuals & reports on engineering practice—No. 42. New York: American Society of Civil Engineers; 1961.

[22] NCHRP report 645, Blast-Resistant Highway Bridges: Design and Detailing Guidelines, Transportation Research Board, Washington D.C. 2010.

[23] Stochino F., Flexural Models of Reinforced Concrete Beams under Blast Load, PhD Thesis, University of Cagliari, 2013.